AIChE

Study on Factors Influencing Stagnation Point Offset of Turbulent Opposed Jets

Wei-Feng Li, Tian-Liang Yao, and Fu-Chen Wang
Key Laboratory of Coal Gasification of Ministry of Education, East China University of Science and Technology, Shanghai 200237, China

DOI 10.1002/aic.12188
Published online January 21, 2010 in Wiley Online Library (wileyonlinelibrary.com).

Turbulent opposed jets were experimentally studied by the hot-wire anemometer measurement, the smoke-wire flow visualization, and the CFD simulation at $L = 1-20D$ (where L is the nozzle separation and D is the nozzle diameter) and $Re > 4500$. The instability pattern of turbulent opposed jets was identified by investigating the smoke-wire photos recorded by a high-speed camera. The factors affecting stagnation point offset, such as the bulk velocity, the velocity profile, and the turbulence intensity at the nozzle exits were investigated. Results show that the stagnation point offset is the main instability regime of turbulent opposed jets. Uniform exit velocity profile and increasing exit turbulence intensity will decrease the stagnation point offset of turbulent opposed jets. © 2010 American Institute of Chemical Engineers *AIChE J,* 56: 2513–2522, 2010

Keywords: turbulent opposed jets, visualization, instability, stagnation point offset, computational fluid dynamics (CFD)

Introduction

Because of rapid and high-effective mixing performance, opposed jets have been applied to a number of industrial processes including coal gasification,[1] mixing,[2,3] drying,[4] SO_2 absorption,[5–7] polymer processing in reaction injection molding (RIM),[8–12] rapid chemical reaction in confined impinging-jets reactor (CIJR),[13–15] etc. However, compared to the numerous applications, fundamental study on the flow characteristics and hydrodynamic instability of turbulent opposed jets is still very limited.

To successfully exploit opposed jets for practical applications, it is important to identify the flow instability pattern and critical parameter influencing stability. Previous studies on the instability of laminar opposed jets are mainly on the transition and the oscillation frequency of the impingement plane. The dynamic behavior of the flow field in RIM has been well studied at $Re < 600$.[8–12] The similar conclusion of these studies is that there exists a critical $Re \approx 90$, above which occurs the flow-field transition from stable laminar to unstable oscillation. The flow visualization in RIM shows that the impingement interface is distorted and displays a sustainable chaotic flow regime by the vortices formed near the impingement point as *Re* is larger than the critical one.[11,12] Stan and Johnson have studied two axisymmetric turbulent opposed water jets in a tank and found that there was an irregular low frequency oscillation (1–20 Hz) for the impingement plane along the symmetric axis.[16] In the experiment of Denshchikov et al., oscillation of two opposed planar water jets at $100 < Re < 4800$ was also observed. The oscillation in their experiment is a deflecting oscillation from the symmetric axis and the two opposed jets are deflected in the opposite directions from each other and switches directions periodically.[17,18]

For two unrestricted turbulent opposed jets, however, several researchers have observed various kinds of stagnation point offset in their experiments. Kostiuk et al. studied turbulent opposed jets using LDA at $L = 2D$ and observed the stagnation point offset along the symmetric axis.[19] In the experiment, they found that a very slight difference of the exit velocities caused the stagnation plane to deviate toward the weaker jet by up to $0.15D$. Lindstedt et al. found that the

Correspondence concerning this article should be addressed to W.-F. Li at liweif@ecust.edu.cn

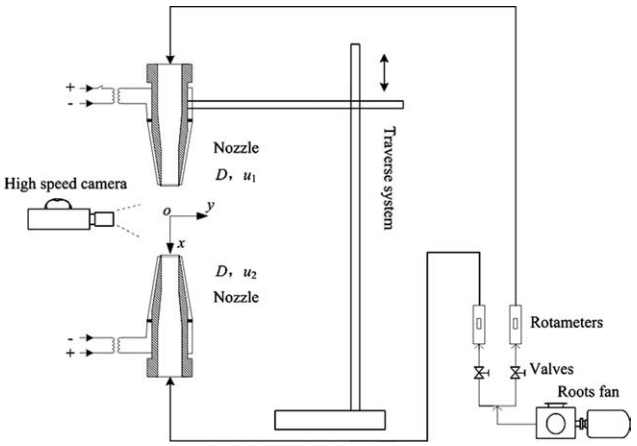

Figure 1. Flowchart of experimental system.

flow was slightly asymmetric in their experiment, and the stagnation point deviated from the symmetry axis by $0.02D$ at $L = 0.4D$.[20] They considered this might arise from the asymmetry of exit velocity profiles. Ogawa and coworkers experimentally studied turbulent opposed jets at $L = 4.3D$ and $8.57D$ and found that double impact positions along the geometric axis could be seen and impingement plane could move to the jet with increasing turbulence.[21,22] Rolon et al. found that there were two stable positions at $Re \approx 1000$ and $L = 1.14D$ when the exit momenta of the opposed jets were equal.[23] In their observations, the two positions are symmetric along the symmetric axis and corresponding to $x = +0.05D$ and $-0.05D$ ($x = 0$ is the center) at $Re \approx 1000$ and $L = 1.14D$, and the two stable flow patterns were mirror images. In our previous study,[24] we have found that in the region of $2D \leq L \leq 8D$, the stagnation point of turbulent opposed jets is very sensitive to the exit velocity ratio, and a slight difference (3% or less) of exit velocities can cause the stagnation point to deviate toward the weaker jet along the axis obviously. Pawlowski et al. performed a fundamental bifurcation and stability analysis of laminar planar and axisymmetric opposed jets. Their study shows that axisymmetric opposed jets exhibit a transition from a single symmetric steady state to three steady states (two stable asymmetric ones and an unstable symmetric one) about at $Re = 60$.[25] Though the stagnation point offset of turbulent opposed jets has been observed and investigated by the above researchers, the instability regime and the factors affecting it is still uncovered. In the industrial application of opposed jets, the flux imbalance is inevitable, and is very crucial to the mixing efficiency and stable operation of the facility in some cases, so study of stagnation point offset is of theory and application importance.

Motivated by the studies cited above, we performed a further study on two turbulent opposed jets at $1D \leq L \leq 20D$ to investigate the stagnation point offset based on our previous work.[24] In the current article, a smoke-wire technique combined with a high-speed camera was used to identify the instability pattern of turbulent opposed jets. Furthermore, influences of the exit velocity profile, the exit bulk velocity, and the exit turbulence intensity on stagnation point offset are investigated.

Experimental Study

Experimental program

The sketch of experiment flowchart is shown in Figure 1. The work fluid was air under normal conditions and was supplied by a roots fan. The flux was controlled by two precision rotameters with accuracy of $\pm 1\%$ of full scale deflection (FSD). The turbulent flow field of opposed jets was obtained by two axisymmetric nozzles with equal geometric configurations, which were precisely aligned in a three-dimensional coordinate frame. Quantitative and qualitative experimental studies of the flow field of the opposed jets were carried out with HWA measurements and the smoke-wire flow visualization.

The exit air velocity ratio of the opposed jets is defined as

$$a = u_2/u_1 \tag{1}$$

where u_1 and u_2 are the exit bulk velocities of upper and lower nozzles, respectively. When the exit velocities of the opposed jets are unequal, the stagnation point will deviate from the mid-point (origin of the coordinate system) between the nozzles. In this case, the distance from the stagnation point to the mid-point is defined as stagnation point offset and denoted by Δx.

Two kinds of nozzles denoted by type A and B were used to produce different degrees of turbulence intensities, as plotted in Figure 2. The exit diameters (D) of the nozzles are 30 mm. The jet Reynolds number at the nozzle exit is defined as

$$Re = Du\rho/\mu \tag{2}$$

where u is the bulk velocity of the jet at the nozzle exit; ρ and μ are the density and dynamic viscosity of air under normal conditions.

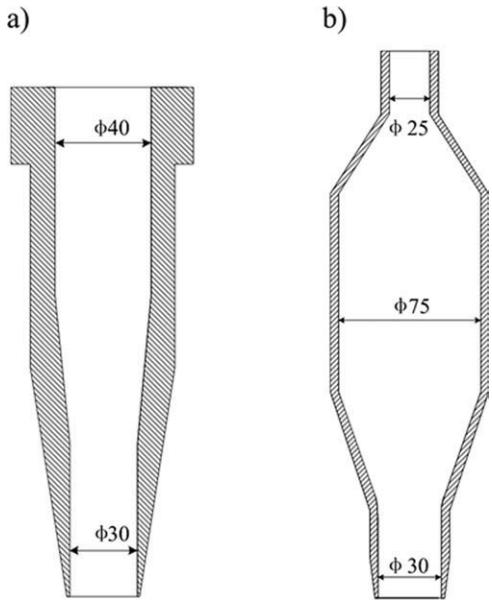

Figure 2. Cross section of the nozzles with all dimensions in millimeters for type A nozzle (a) and type B nozzle (b).

Table 1. Cases of Flow Visualization

L/D	u_1 (m/s)	a	Re_1	Re_2
1, 2, 4, 6, 8, 12	2.36	1, 0.97	4692	4551–4692

Smoke-wire technique

The instantaneous flow patterns of turbulent opposed jets were visualized by a smoke-wire technique with a high-speed camera, as shown in Figure 1. A 0.1 mm diameter stainless steel wire was located across the nozzle exit. The wire was coated by the paraffin oil and connected as a resistor to an electric circuit. Then, the oil was heated to form smoke by the sudden current when the circuit was on. A high-speed camera (Photron APX-RS, up to 3000 frames per second with full resolution 1024 × 1024 pixels) was used in combination with a continuous 2000 W direct current light to capture the pictures of the smoke-wire. The resolution of the picture was 1024 × 1024 pixels and the exposure time was 0.001 s. The sampling time of the high-speed camera was set at 3 s and can record the entire duration of the smoke-wire from startup to disappearance. The experimental cases of the flow visualization are listed in Table 1.

Hot-wire anemometer measurement

Mean and root mean square (RMS) velocities of the turbulent flow field of the opposed jets were measured with a DANTEC hot-wire anemometry system. The stagnation point was identified by measuring the velocity distribution along the axis and the position with the minimum velocity was considered as the stagnation point. The probe connected to the frame of the HWA has a single wire. The sampling frequency was set at 20 kHz and the sampling duration was 5 s. In the measurements, the nozzle separation L is in the region of 30–600 mm and the corresponding normalized nozzle separations L/D range from 1 to 20. The detailed measurement cases are listed in Table 2.

Numerical simulation and verification

To investigate the influence of the exit velocity profile on the stagnation point offset of turbulent opposed jets, a numerical simulation of the flow of opposed jets with uniform exit velocity profile was carried out. The simulation was performed using a microcomputer and available CFD commercial software (Fluent 6.1). The flow field of turbulent opposed jets was solved as a two-dimensional axisymmetric flow using the finite volume method. The coordinate system, computation domain, and boundary conditions are similar to the simulation in our previous article.[24] Standard k–ε and RNG k–ε models and RSM were selected to simulate the flow of turbulent opposed jets.

The simulation method stated above was verified by the available LDV measurements of Kostiuk et al.[19] In their experiment, the nozzle diameter D and the nozzle separation L are 35 mm and 55 mm and the exit bulk velocity and normalized RMS velocity are 8.7 m/s and 7%. It must be mentioned that the nozzles used in their experiment were especially designed to produce uniform exit velocity profile. To simulate this flow, a uniform velocity inlet was adopted. Figure 3 shows the simulated axial velocity distribution of the LDV measurements in the literature.[19] All of the three turbulence models can predict mean velocity distribution satisfactorily and the discrepancy between simulation and experiment is less than 5%, which proves the numerical simulation method in current study is reasonable.

Champion and Libby presented an analytic solution of the turbulence flow issuing from two closely opposed jets based on the Reynolds stress description.[26] According to their analytic solution, the axial velocity distribution of axisymmetric opposed jets is described as

$$u = -\frac{4u_0 x}{L}\left(1 - \frac{x}{L}\right), \quad x > 0$$

and

$$u = -\frac{4u_0 x}{L}\left(1 + \frac{x}{L}\right), \quad x < 0 \tag{4}$$

where u_0 is the exit bulk velocity and x is the axial coordinate. We used Eq. 4 to calculate the axial velocity of Kostiuk et al.[19] The calculated result is also plotted in Figure 3a. It is seen that the calculated result is completely coincident with the experimental and numerical ones, which proves that the analytic solution in Eq. 4 can predict mean velocity well when the exit velocity profiles of the turbulent opposed jets are uniform.

The simulated turbulence intensity distribution on the axis by three turbulence models and experimental values are plotted in Figure 3b. It is shown that none of the turbulence models can predict the RMS velocities perfectly. Especially, in the impingement region, the RMS velocities were overestimated by factors of 1.2, 1.4, and 2 by the RNG k–ε, RSM, and Standard k–ε models. Comparatively, the RSM is more acceptable than the other two ones. So, in the following sections of this article, the RSM model was used to simulate the flow of turbulent opposed jets.

Results and Discussion

Flow pattern of turbulent opposed jets

With the smoke-wire photos recorded by the high-speed camera, we can observe the instability pattern of turbulent opposed jets conveniently. In the flow visualization, u_1 is fixed at 2.36 m/s and exit velocity ratios are 0.97 and 1 ± 1%, where 1% is added because the precision of the flux control is about ±1% in current experiment. From the smoke-wire images, the first feature is that in all of our experiment cases, no oscillation of the impingement plane

Table 2. Measurement Cases

L/D	u_1 (m/s)	a	Re_1	Re_2
1, 2, 4, 6, 8, 12, 16, 20	2.36–11.8	1, 0.97, 0.9, 0.8, 0.7	4692–23460	4551–22756

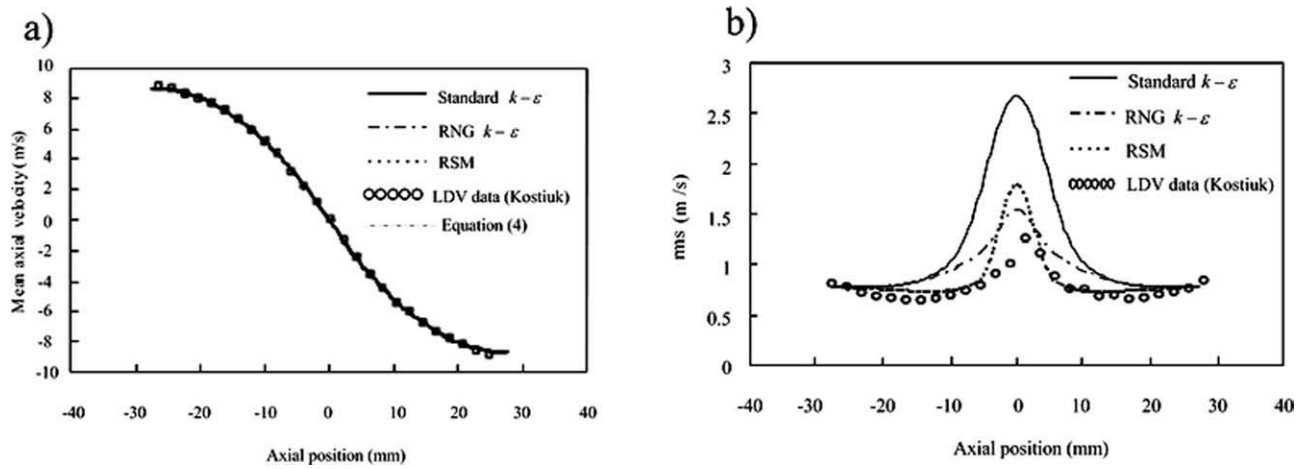

Figure 3. Simulation and analytic solution of axial mean velocity (a) and RMS velocity (b) of LDV data in the literature.[19]

was observed. The selected typical photographs for $L = 4D$ are presented in Figure 4, and more smoke-wire photos by digital camera can be seen in our previous work.[24] At $L = 4D$, it is very interesting to observe that the impingement plane stays at the positions near to either the upper nozzle or the lower nozzle, as shown in Figures 4a, b. It is impossible to get the impingement stagnation point stay at the midpoint even with enough patience by adjusting the flux balance. When there is a slight difference of exit velocities, the impingement plane will deviate from the midpoint dramatically, as shown in Figure 4c. It should be noted that the stagnation point offset values in the three figures are all about $1.33D$.

Simulated vector maps of opposed jets at $L = 4D$ and various exit air velocity ratios are shown in Figure 5. Result indicates that the stagnation point is located at the geometric center and the impingement plane is vertical to the axis at $a = 1$. At $a = 0.97$, the stagnation point shifts toward the lower jet and its offset is $1.33D$, which is in good agreement with the visualization results. Though the simulation in current work used a steady solver of Fluent, the vector maps at $a = 0.995$ and 1.005 are very meaningful, as shown in Figures 5c, d. In the figures, only exit velocity difference of 5‰ causes the stagnation point to deviate to the positions very close to the upper and lower nozzles, and their offset values are also $+1.33D$ and $-1.33D$, respectively. The simulation results are still consistent with the observations in current article and literature that very slight exit velocity difference can cause the stagnation point to deviate from the center significantly.[19,24]

Above visualization and simulation indicate that the flow of turbulent opposed jets is an unstable system, which is subjected to the disturbance such as flux fluctuation and the stagnation point will deviate from the geometric center and along the symmetry axis. In all of our experiment cases, no oscillation was observed, and the stagnation point offset is the dominant instability regime for turbulent opposed jets. It must be mentioned that current study is only focused on the instability of the impingement plane or stagnation point on the axis. The instability of the radial jet formed by the opposed jets is out of the scope of current study, though large vortexes and flapping of the radial jet can be observed. The instability pattern of turbulent opposed jets can be described by Figure 6 schematically, in which the two positions denoted by dot are semi-stable but the mid-point denoted by square is unstable, and the region between the two semi-stable points is unstable too. Here, the term "semi-stable" means the stagnation point at that position is easy to move to another semi-stable position but is hard to move toward the jet exits. The instability regime observed in current study is similar to Rolon et al.[23] and Pawlowski et al.,[25] though the flows in their work are laminar. But current instability regime is different to the deflecting oscillation instability in RIM and planar opposed jets,[8–12,17,18] which may be due to the influences of the wall or the nozzle geometry.

From the previous description, it is seen that the instability of turbulent opposed jets behaves as the deviation of the stagnation point form the center. It must be pointed out that only at $L = 4D$, the stagnation point of turbulent opposed jets with equal exit velocities cannot be located at the center,

Figure 4. Smoke-wire photos at $L = 4D$, $a = 1 \pm 1\%$ (a and b) and 0.97 (c).

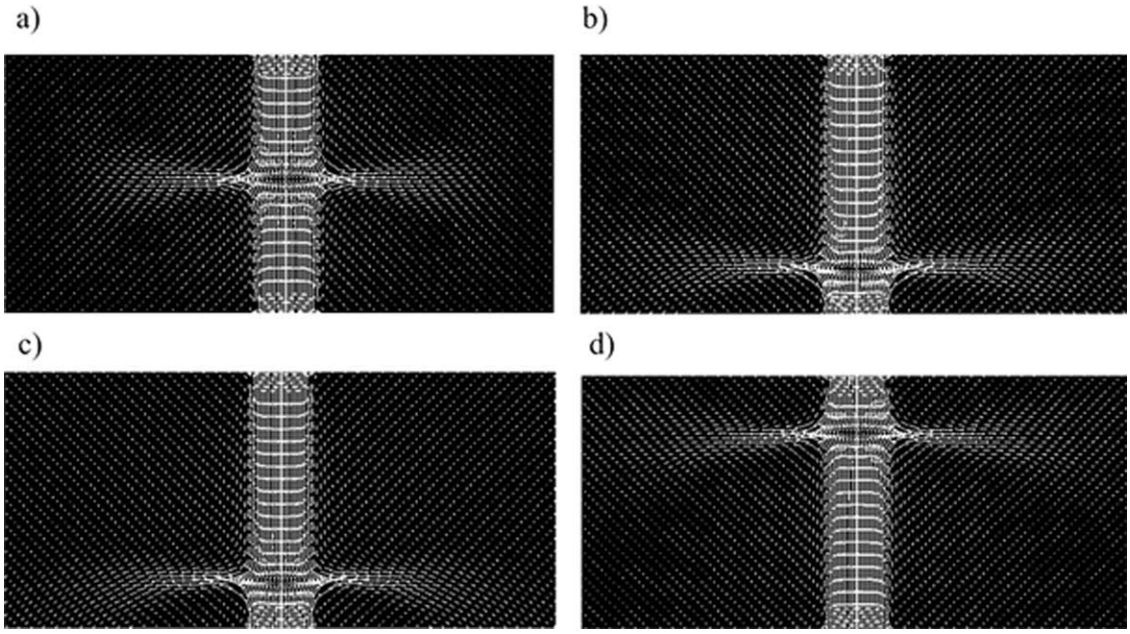

Figure 5. Simulated vector maps at $L = 4D$, $a = 1$ (a), 0.97 (b), 0.995 (c), and 1.005 (d).

and at other nozzle separations, the stagnation point can stay at the center if we control the flux with more or less patience. When there is a slight difference of the exit momenta, different degrees of stagnation point offset can be observed, which implies the sensitivity and instability of the impingement plane of turbulent opposed jets have close relationship to the nozzle separation. So, the stagnation point offset when there is a slight difference of the exit momenta is the manifestation of the instability to a certain extent. The stagnation point offset at $a = 0.97$ is obtained by investigating the smoke-wire photos at various nozzle separations, as shown in Figure 7. In the figures, the stagnation point offset is normalized by nozzle diameter and nozzle separation, respectively. With the increase of nozzle separations, the stagnation point offset increases sharply, and reaches maximum at $L = 4D$, then decreases gradually at $L > 4D$.

Factors affecting stagnation point offset of turbulent opposed jets

In the previous section, the stagnation point offset caused by the flux imbalance at various nozzle separations has been discussed, and other factors affecting the stagnation point offset, such as exit velocity profiles, exit bulk velocities, and exit turbulence intensities will be investigated further in the following sections. Results corresponding to $a = 0.97$ are also represented in separate figures to indicate the sensitivity of stagnation point offset to the slight difference of exit velocities under various conditions.

Effect of exit velocity profile on stagnation point offset

The normalized axial mean and RMS velocity profiles of type A and B nozzles are plotted in Figure 8, in which the curves are measured at 1 mm of the free jet exit. It is seen that the nozzles have "top-hat" exit velocity profiles and mean velocity profiles are flat for more than 80% of the nozzle diameter D and the thickness of the boundary layer at the jet exit is about $0.1D$. The figure shows that the two types of nozzles have similar shape of exit velocity profiles but the turbulence intensities of them are about 4.3% and 12%, which is due to their different geometry configurations.

Because opposed jets with uniform exit velocity profiles are very difficult to obtain in our experiments, simulations were carried out for turbulent opposed jets with uniform exit velocity profiles. In the simulation, the exit bulk velocity and turbulent intensity of the jets with uniform exit velocity profiles were set to be same to the "top-hat" jets. The measured results of stagnation pint offset of opposed jets with "top-hat" nozzles and the simulated ones with uniform nozzles are shown in Figure 9 and the values corresponding to $a = 0.97$ are presented in Figure 10. It can be seen in Figure 9 that the stagnation point offset of opposed jets with uniform nozzles is obviously smaller than that with "top-hat" nozzles. Figure 10 indicates that the stagnation point of opposed jets with "top-hat" nozzles is more sensitive to the slight

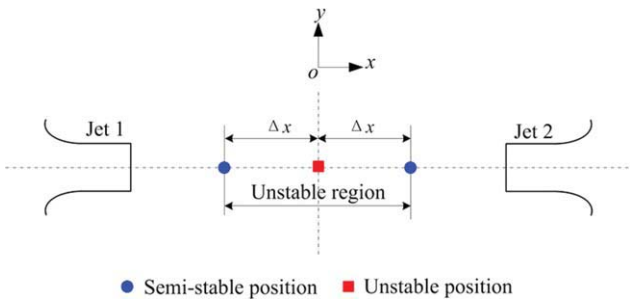

Figure 6. Schematic representation of instability of turbulent opposed jets.

[Color figure can be viewed in the online issue, which is available at wileyonlinelibrary.com.]

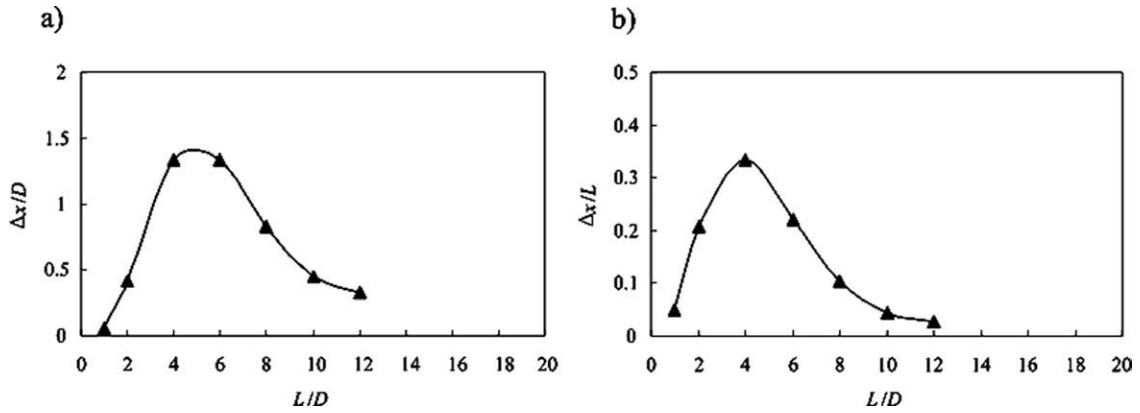

Figure 7. Stagnation point offset obtained from smoke-wire photos and normalized by *D* (a) and *L* (b) of turbulent opposed jets at u_1 = 2.36 m/s and a = 0.97.

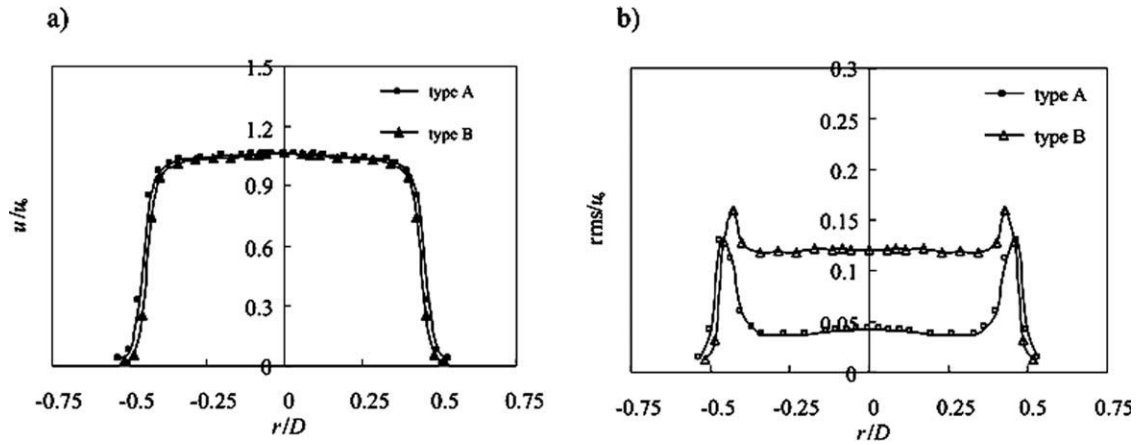

Figure 8. Mean (a) and RMS (b) velocity profiles of free jets with type A and B nozzles at u_0 = 11.8 m/s.

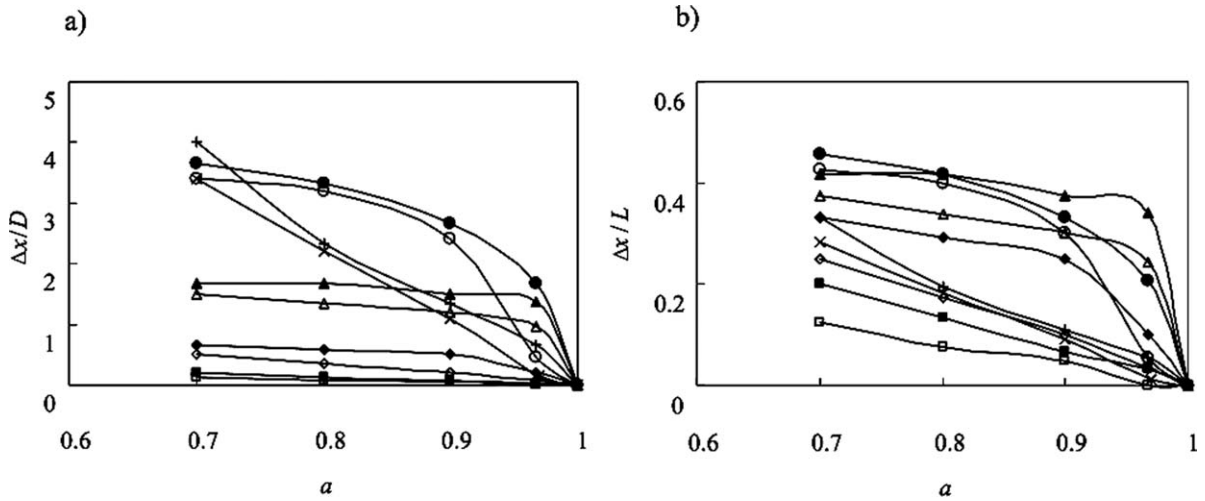

Figure 9. Stagnation point offset of opposed jets with top-hat and uniform exit velocity profiles at u_1 = 11.8 m/s.

Top-hat, experiment: ■, 1*D*; ◆, 2*D*; ▲, 4*D*; ●, 8*D*; +, 12*D*; Uniform, simulation: □, 1*D*; ◇, 2*D*; △, 4*D*; ○, 8*D*; ×, 12*D*.

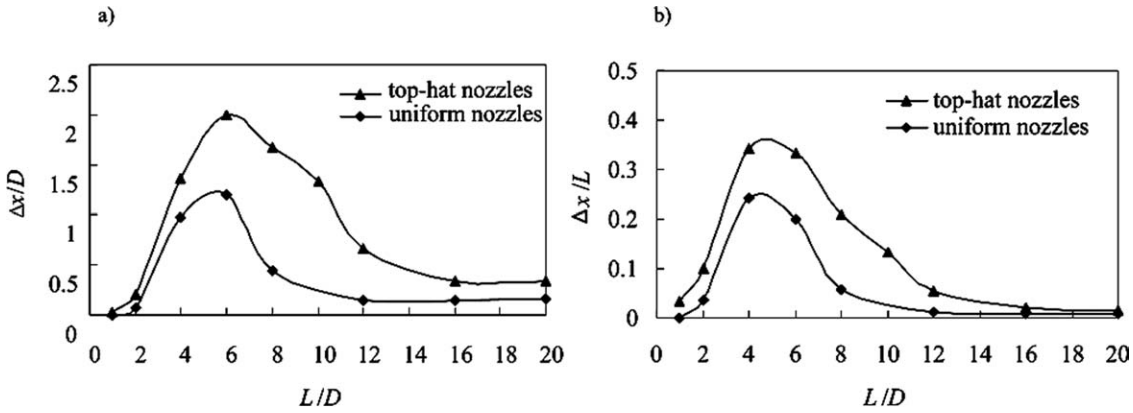

Figure 10. Measured and simulated stagnation point offset normalized by *D* (a) and *L* (b) of opposed jets with top-hat and uniform profiles at $a = 0.97$ and $u_1 = 11.8$ m/s.

difference of exit velocities than that with "top-hat" nozzles. The initial boundary layer thickness of the jet with a "top-hat" exit velocity profile is larger than that with a uniform profile. The difference in the figures indicates that the increasing boundary layer thickness at the jet exit increases the stagnation point offset of turbulent opposed jets.

Effect of exit bulk velocity on the stagnation point offset

To investigate the influence of exit bulk velocities on stagnation point offset, two magnitudes of u_1 (2.36 m/s and 11.8 m/s) are studied and the results are shown in Figures 11 and 12. In Figure 11, the values for $u_1 = 2.36$ m/s and 11.8 m/s are experimental measurements. In Figure 12, the simulation values for $u_1 = 11.8$ m/s are also represented. Considering the sensitivity of the stagnation point to the slight exit velocity difference in the experiment, the simulation is generally in agreement with the experimental measurements. More detailed comparison between experimental measurements and simulations of the stagnation point offset can be found in our previous work.[24] The influence of the exit bulk velocity on stagnation point offset is complicated: at $L < 4D$, with the increase of exit bulk velocities, the stagnation point offset decreases slightly; however, at $L > 4D$, the stagnation point offset increases from 2.36 m/s to 11.8 m/s, as shown in Figure 12. $L = 4D$ is the turning point at which the exit bulk velocity has little influence on stagnation point offset. This is due to the fact that at $L = 4D$, the stagnation point offset is very large already.

Effect of exit turbulence intensity on stagnation point offset

In this section, the influence of the exit turbulence intensity on the stagnation point offset of turbulent opposed jets is investigated. Two kinds of nozzles with different exit turbulence intensities are applied and their exit mean and RMS velocity profiles are shown in Figure 8. The results of stagnation point offset with different exit turbulence intensities are shown in Figures 13 and 14. The figures show that the stagnation point offset at $I = 12\%$ is significantly smaller than that at $I = 4.3\%$. Smoke-wire photos of opposed jets with $I = 12\%$ are presented in Figure 15. It is shown that at $L = 4D$, the impingement plane can stay at the center when the exit bulk velocities are identical, and at $a = 0.97$, the stagnation point offset is only about $0.8D$.

From the previous discussion, it can be seen that increased exit turbulence intensity can stabilize the impingement plane

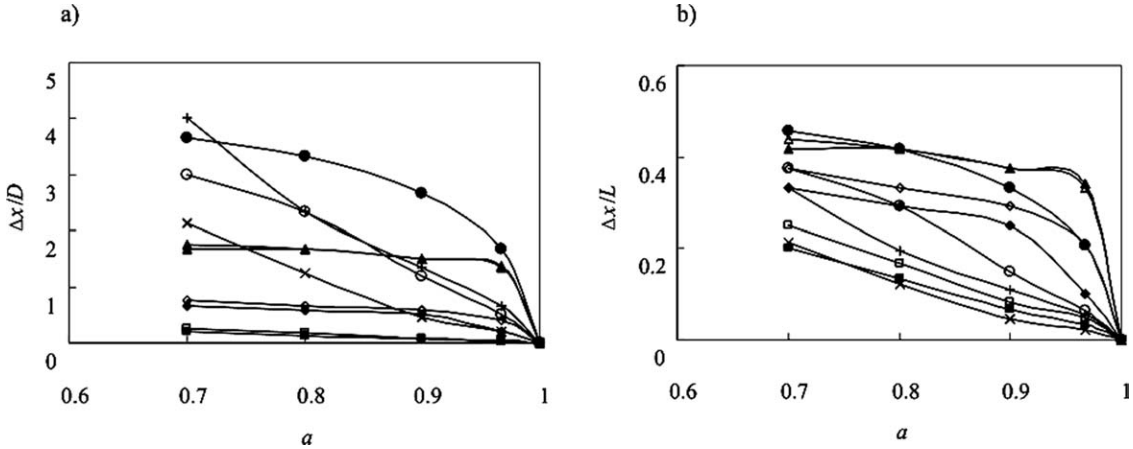

Figure 11. Measured stagnation point offset of opposed jets with different exit bulk velocities.

$u_1 = 11.8$ m/s: ■, 1*D*; ◆, 2*D*; ▲, 4*D*; ●, 8*D*; +, 12*D*; $u_1 = 2.36$ m/s: □, 1*D*; ◇, 2*D*; △, 4*D*; ○, 8*D*; ×, 12*D*.

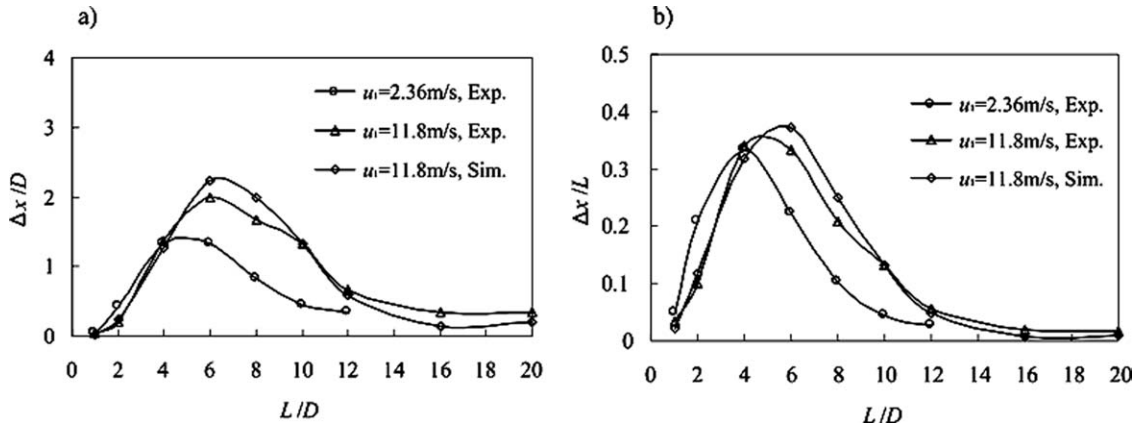

Figure 12. Stagnation point offset normalized by *D* (a) and *L* (b) at various exit bulk velocities and $a = 0.97$.

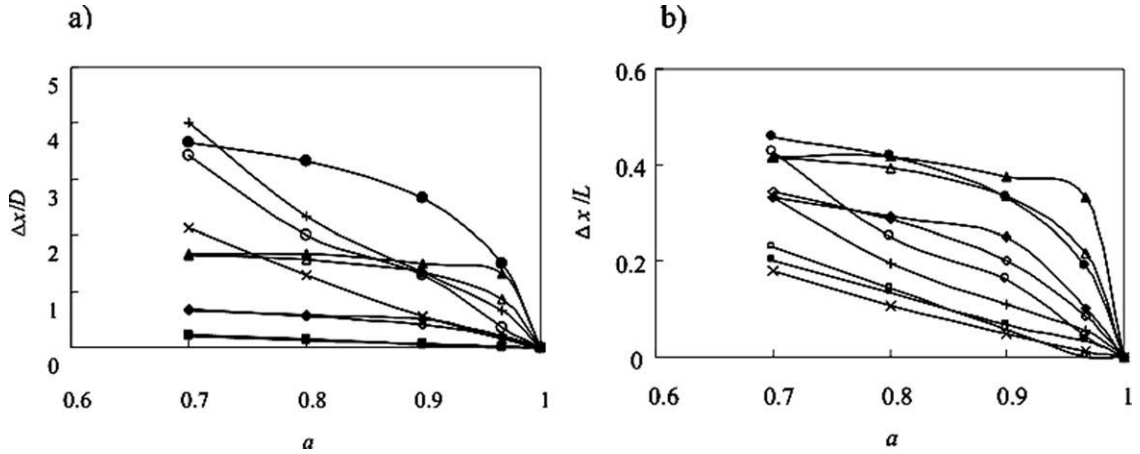

Figure 13. Measured stagnation point offset of opposed jets with different exit turbulence intensities at $u_1 = 11.8$ m/s.

Type A nozzle: ■, 1*D*; ◆, 2*D*; ▲, 4*D*; ●, 8*D*; +, 12*D*; Type B nozzle: □, 1*D*; ◇, 2*D*; △, 4*D*; ○, 8*D*; ×, 12*D*.

of turbulent opposed jets to some extent. By comparing the smoke-wire photos in Figures 4 and 15, we can observe that the scales of the large-scale vortexes are different in the boundary layers of jets formed by the two kinds of nozzles. The higher the turbulence intensity, the smaller the scale of the vortex is. In previous study, we presumed that large-scale instability in the boundary layer caused the different stagnation point offset at various nozzle separations.[24]

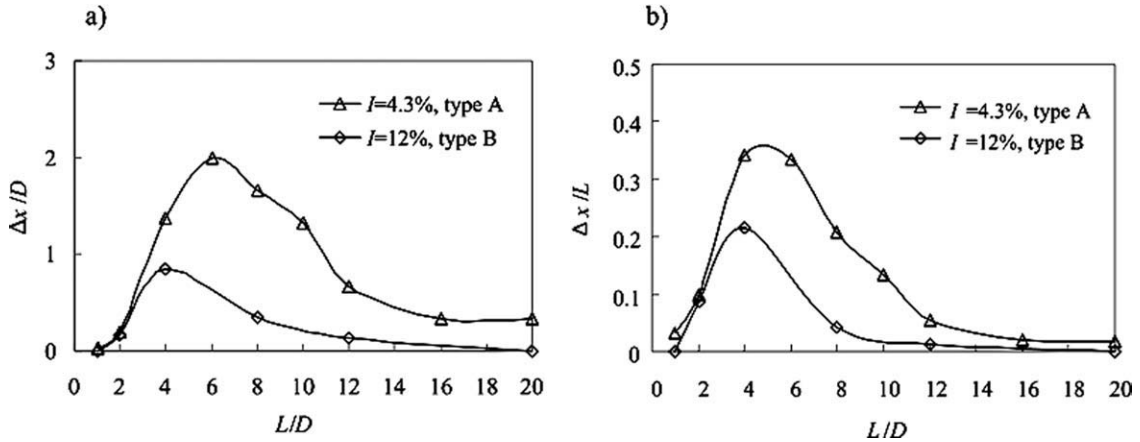

Figure 14. Measured stagnation point offset normalized by *D* (a) and *L* (b) of opposed jets at $u_1 = 11.8$ m/s and $a = 0.97$.

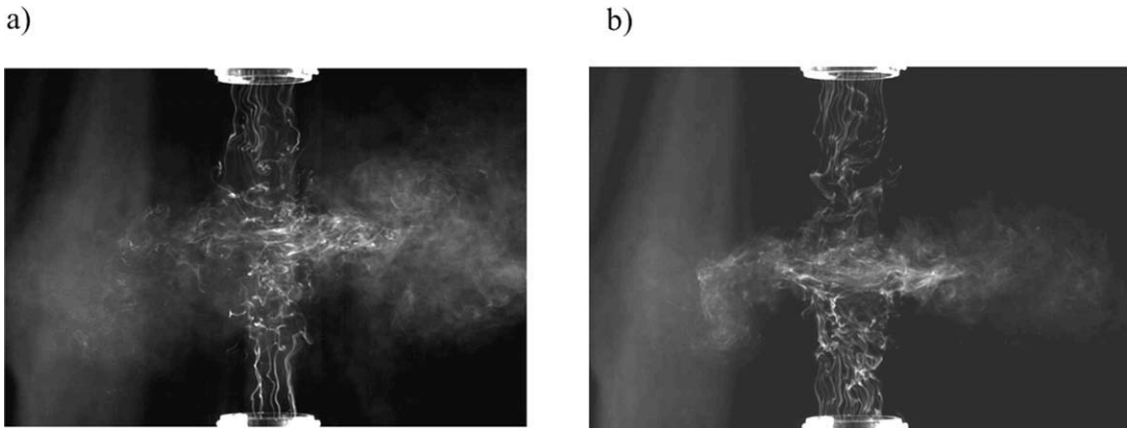

Figure 15. Smoke-wire photos of opposed jets at $L = 4D$, $u_1 = 2.36$ m/s, $I = 12\%$, $a = 1 \pm 1\%$ (a) and 0.97 (b).

Current study further confirms that the large-scale instability has strong influence on the stagnation point offset and the instability of turbulent opposed jets.

The stagnation point offset results for turbulent opposed jets in the literature are very few, and the only few results are not comparable, because they are obtained under various nozzle separations and different exit conditions of the jets. Present study manifests that besides the exit velocity ratio and nozzle separation, jet exit conditions, such as the exit velocity profile, the exit Reynolds number and the exit turbulence intensity also have significant influences on the stagnation point offset, especially in the region of $2D < L < 8D$.

Conclusions

The study of the stagnation point offset of impinging streams is crucial for the effective application of such flow in industry. The flow of turbulent opposed jets at $Re > 4500$ and $1D \leq L \leq 20D$ were studied in current study. Instability regimes of turbulent opposed jets were identified and the influences of exit velocity profiles, exit bulk velocities, and exit turbulence intensities on the stagnation point offset have been investigated. The main conclusions can be summarized as follows.

(1) The stagnation point offset is the dominant instability regime for turbulent opposed jets, and no oscillation is observed. At $L = 4D$, the stagnation plane is very unstable and can only stay at the two semi-stable positions, which are very close to the jet exits.

(2) Jet exit conditions, such as the exit velocity profile, the exit Reynolds number, and the exit turbulence intensity, have influence on the stagnation point offset, especially in the region of $2D < L < 8D$. The uniform exit velocity profile or increasing turbulence intensity will decrease the stagnation point offset and can stabilize the flow of turbulent opposed jets.

Acknowledgments

This study was supported by the National Development Programming of Key Fundamental Researches of China (2010CB227004) and the Natural Science Foundation of China (20906024). Especially, the authors add their thanks to the anonymous reviewers for their helpful suggestions on the quality improvement of their article.

Notation

a = exit velocity ratio
D = nozzle diameter
L = nozzle separation
I = turbulence intensity
Re = jet Reynolds number
u, u_0, u_1, u_2 = axial velocity
x, y = axial, radial coordinate
ρ = air density
μ = dynamic viscosity of air
Δx = stagnation point offset

Literature Cited

1. Wang FC, Zhou ZJ, Dai ZH, Gong X, Yu GS, Liu HF, Wang YF, Yu ZH. Development and demonstration plant operation of an opposed multi-burner coal-water slurry gasification technology. *Front Energy Power Eng China*. 2007;1:251–258.
2. Devahastin S, Mujumdar AS. A numerical study of flow and mixing characteristics of laminar confined impinging streams. *Chem Eng J*. 2002;85:215–223.
3. Niamnuy C, Devahastin S. Effects of geometry and operating conditions on the mixing behavior of an in-line impinging stream mixer. *Chem Eng Sci*. 2005;60:1701–1708.
4. Hosseinalipour SM, Mujumdar AS. Superheated steam drying of a single particle in an impinging streams dryer. *Drying Technol*. 1995;13:1279–1303.
5. Berman Y, Tanklevsky A, Oren Y, Tamir A. Modeling and experimental studies of SO_2 absorption in coaxial cylinders with impinging streams: part I. *Chem Eng Sci*. 2000;55:1009–1021.
6. Berman Y, Tanklevsky A, Oren Y, Tamir A. Modeling and experimental studies of SO_2 absorption in coaxial cylinders with impinging streams: part II. *Chem Eng Sci*. 2000;55:1022–1032.
7. Wu Y, Li Q, Li F. Desulfurization in the gas-continuous impinging stream gas-liquid reactor. *Chem Eng Sci*. 2007;62:1814–1824.
8. Wood PE, Hrymak A, Yeo R, Johnson DA, Tyagi A. Experimental and computational studies of the fluid mechanics in an opposed jet mixing head. *Phys Fluids A*. 1991;3:1362–1368.
9. Johnson DA, Wood PE. Self sustainable oscillations in opposed impinging jets in an enclosure. *Can J Chem Eng*. 2000;78:867–875.
10. Teixeira AM, Santos RJ, Costa MRPFN, Lopes JCB. Hydrodynamics of the mixing head in RIM: LDA flow-field characterization. *AIChE J*. 2005;51:1608–1619.

11. Santos RJ, Erkoç E, Dias MM, Teixeira AM, Lopes JCB. Hydrodynamics of the mixing chamber in RIM: PIV flow-field characterization. *AIChE J*. 2008;54:1153–1163.
12. Santos RJ, Erkoç E, Dias MM, Lopes JCB. Dynamic behavior of the flow field in a RIM machine mixing chamber. *AIChE J*. 2009;55:1338–1351.
13. Johnson BK, Prud'homme RK. Chemical processing and micromixing in confined impinging jets. *AIChE J*. 2003;49:2264–2282.
14. Liu Y, Fox RO. CFD predictions for chemical processing in a confined impinging-jets reactor. *AIChE J*. 2006;52:731–744.
15. Gavi E, Marchisio DL, Barresi AA. CFD modeling and scale-up of confined impinging Jet reactors. *Chem Eng Sci*. 2007;62:2228–2241.
16. Stan G, Johnson DA. Experimental and numerical analysis of turbulent opposed impinging jets. *AIAA J*. 2001;39:1901–1908.
17. Denshchikov VA, Kontratev VN, Romashev AN. Interaction between two opposed jets. *Fluid Dyn*. 1978;6:924–926.
18. Denshchikov VA, Kontratev VN, Romashev AN, Chubarov VM. Auto-oscillations of planar colliding jets. *Fluid Dyn*. 1983;3:460–462.
19. Kostiuk LW, Bray KNC, Cheng RK. Experimental study of premixed turbulent combustion in opposed streams. Part I: Nonreacting flow field. *Combust Flame*. 1993;92:377–395.
20. Lindstedt P, Luff DS, Whitelaw JH. Velocity and strain-rate characteristics of opposed isothermal flows. *Flow. Turbul Combust*. 2005;74:169–194.
21. Ogawa N, Maki H. Studies on opposed turbulent jets (Influences of a body on the axis of opposed turbulent jets). *Bull JSME*. 1986;29:2872–2877.
22. Ogawa N, Maki H, Hijikata K. Studies on opposed turbulent jets (Impact position and turbulent component in jet center). *Int J JSME*. 1992;35:205–217.
23. Rolon JC, Veynante D, Martin JP. Counter jet stagnation flows. *Exp Fluids*. 1991;11:313–324.
24. Li WF, Sun ZG, Liu HF, Wang FC, Yu ZH. Experimental and numerical study on stagnation point offset of turbulent opposed jets. *Chem Eng J*. 2008;138:283–294.
25. Pawlowski RP, Salinger AG, Shadid JN, Mountziaris TJ. Bifurcation and stability analysis of laminar isothermal counterflowing jets. *J Fluid Mech*. 2006;551:117–139.
26. Champion M, Libby PA. Reynolds stress description of opposed and impinging turbulent jets. Part I: closely spaced opposed jets. *Phys Fluids A*. 1993;5:203–216.

Manuscript received Apr. 26, 2009, revision received Nov. 1, 2009, and final revision received Jan. 15, 2010.